FDC Prototype Studies

Simon Taylor and Daniel S. Carman
Department of Physics, Ohio University, Athens, OH 4570

March 24, 2005

Abstract

Preliminary results from studies of the first small-scale FDC prototype are presented. Both cathode planes are used to reconstruct the wire positions. The Gaussian resolution of the reconstructed wire positions is currently about 220–250 μm.

We report on the current status of the FDC cathode strip chamber development. A sketch of a typical cathode strip chamber is shown in figure 1. The anode wire pitch is s, the cathode strip pitch is w, the strip-to-strip gap is g, and the half-gap (anode-to-cathode separation) is h.

We constructed a prototype consisting of cathode and anode layers that could be easily swapped out so that we could study various electrode configurations. The active area of the prototype is about 7"$\times$7". The wire planes consisted of sixteen 20 micron diameter sense wires set at a 10 mm pitch. We made one with field-shaping wires offset by 5 mm from the sense wires and one without. The cathodes were made from Kapton layers with copper strips set at a 5 mm pitch with either $\pm 45^\circ$ orientation with respect to the wires or perpendicular orientation with respect to the wires. The gap between the cathode strips is another parameter we varied. We constructed cathode planes with g=0.25 mm, 0.5 mm, and 1.0 mm. The cathode-anode separation h was fixed to 5 mm. The results for the first incarnation of the prototype, in which only the sense wires were present, the strips were oriented at $\pm 45^\circ$ with respect to the wires, and the strip-to-strip gap was set to $g = 1$ mm, will be presented in this article. A sketch of this geometry is shown in figure 2.

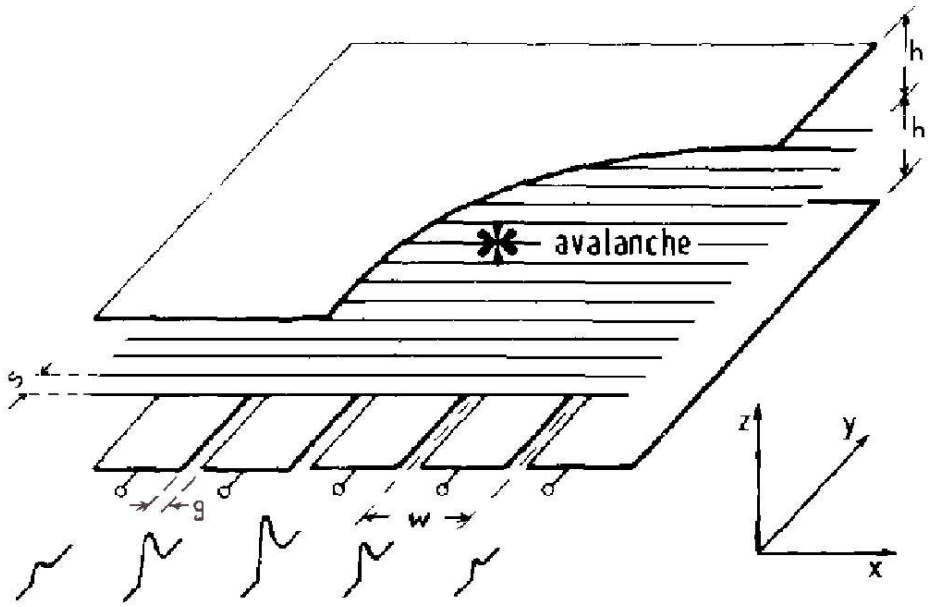

Figure 1: Geometry of a typical cathode strip chamber (figure adapted from [1]).

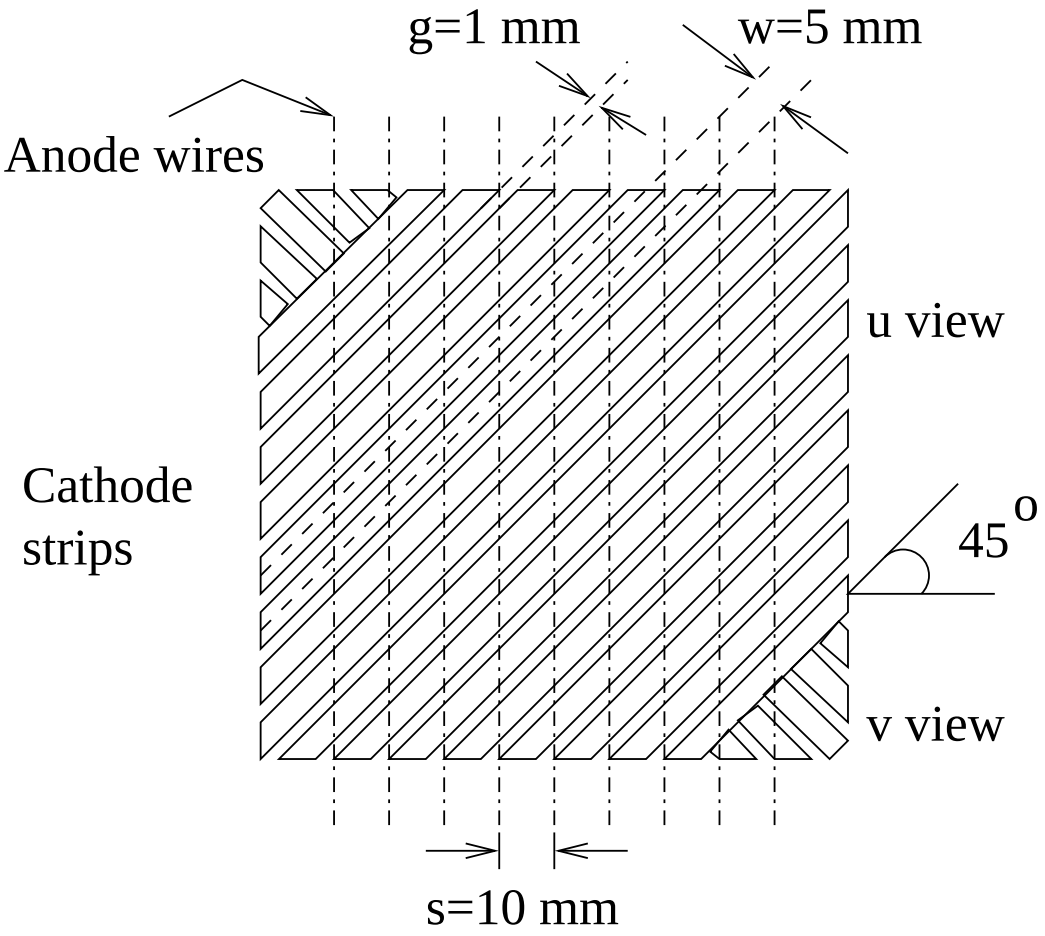

Figure 2: Sketch of geometry for prototype configuration under study for this article.

A photograph of the assembled prototype is shown in figure 4. Both the cathode and anode signals are amplified at the prototype with SIPs used in the Hall-B drift chamber design. A schematic diagram of the on-chamber components is shown in figure 3. The differential signals produced by the preamplifiers are converted to single-ended negative-going signals by VPI postamplifiers with gains of roughly unity. The primary purposes of the postamplifiers were to match impedances and to provide the correct pulse polarity for the CAMAC and FASTBUS electronics in the readout. The gains were crudely calibrated in hardware from channel to channel using an oscilloscope and later in software by injecting charge into the test inputs of the preamplifiers and aligning the resulting peaks after performing a channel-by-channel pedestal subtraction. The output of the postamplifiers then passes to the readout electronics for the cathodes and a CAMAC discriminator for the anode signals. The sense wires were biased at +1760 V; the cathode layers were at ground potential. We used a premixed gas consisting of 90% Argon and 10% CO_2. A drift line plot generated using Garfield for this electrode configuration and gas mixture is shown in figure 5.

In order to study the prototype's performance, we constructed a cosmic ray telescope consisting of two scintillators placed above and below the prototype and four larger multi-wire drift chambers (MWDCs) to define tracks for cosmic rays passing through the prototype. The coordinate system we have used was such that the y-direction was along the wires and the x-direction was transverse to the wires. The scintillator geometry allows for an angular range of the incident muons of about 10° in the x-direction and 17° in the y-direction relative to vertical incidence. A photograph of the setup is shown in figure 6 and a schematic diagram is shown in figure 7. A coincidence between signals in the top scintillator and in the bottom scintillator provides the trigger for the data acquisition system. The timing signals from the chambers are digitized with a Lecroy 1877 TDC operating in common-stop mode. The delayed signal from the scintillator coincidence provides the stop. The analog signals from the cathode strips are read out with a Lecroy 1881M ADC. Again, the scintillators are used to define the beginning of the gate for the ADC.

For a single muon passing through the prototype chamber, each cathode plane should see the same amount of induced charge from the resulting avalanche. This expectation is borne out by the data (figure 8), where the ADC values are summed over 7 adjacent cathode strips containing the maximum in each view (seven was chosen because most peaks are contained within

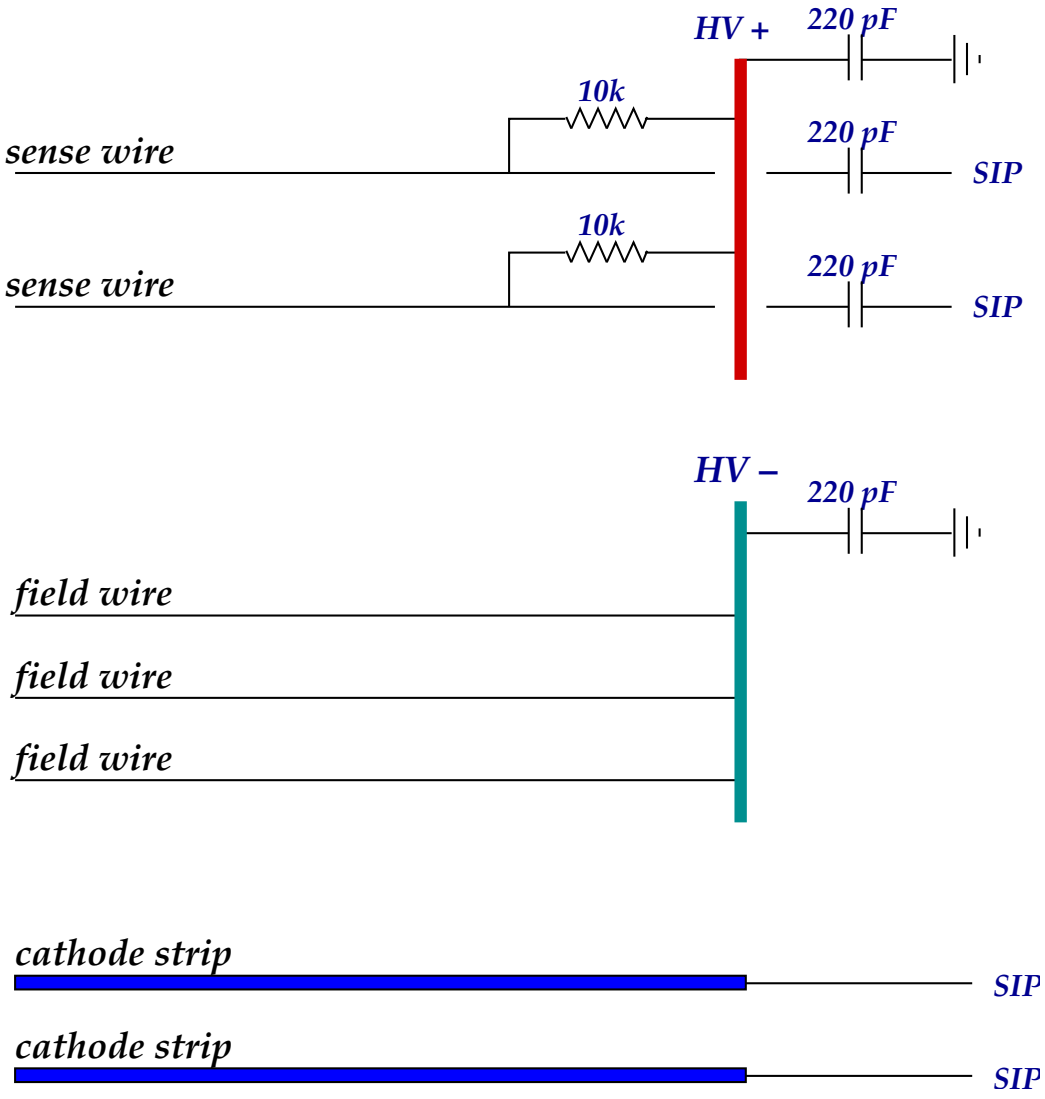

Figure 3: Schematic diagram of the on-chamber anode and cathode readout electronics.

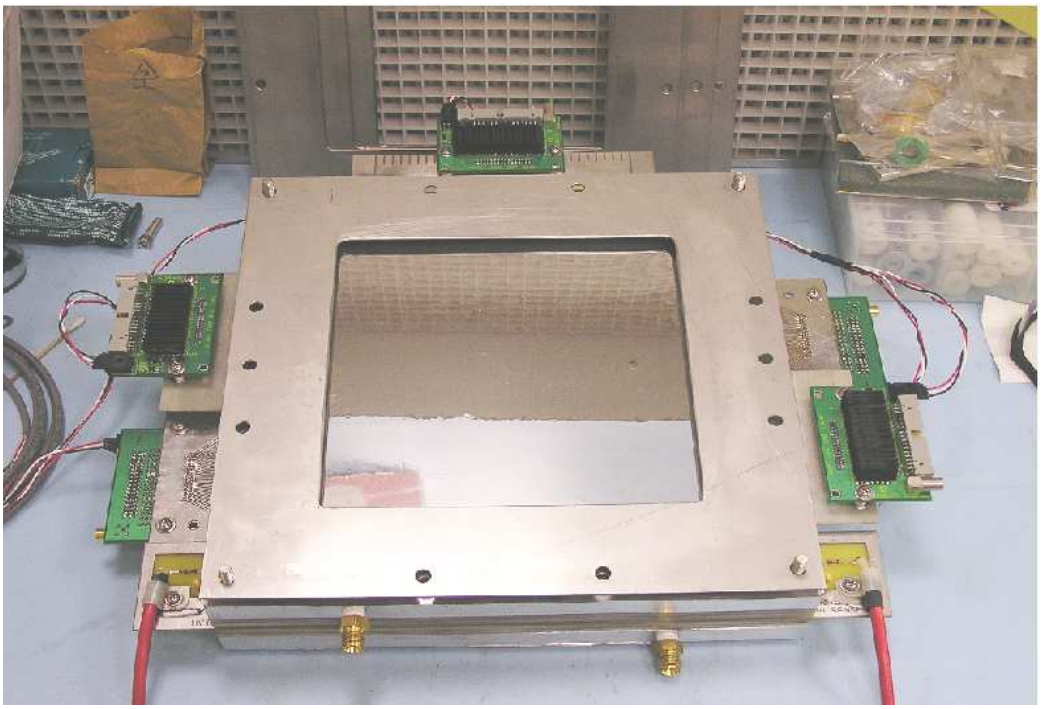

Figure 4: Photograph of assembled FDC prototype.

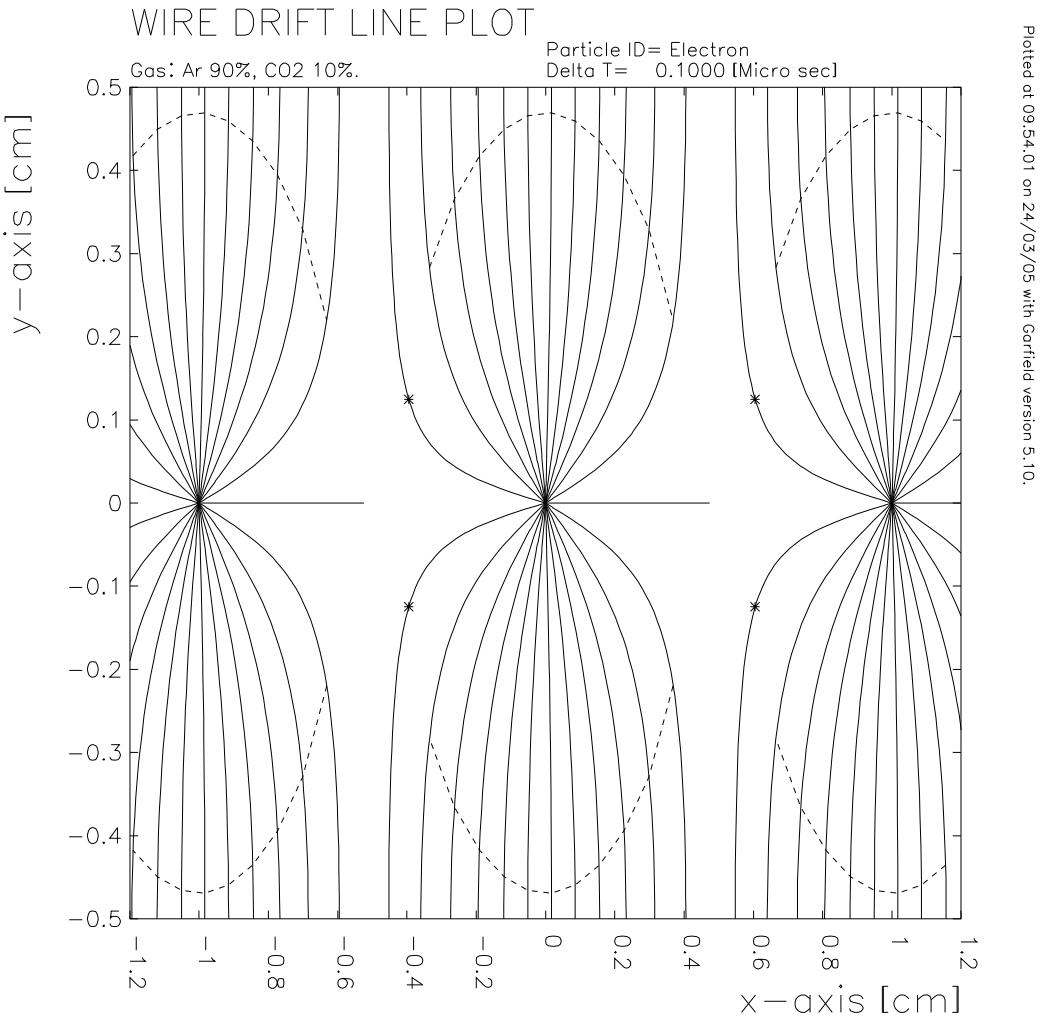

Figure 5: Garfield calculation of drift lines for sense wires at +1760 V separated by 10 mm. The wires are at x=0 and ±1 cm; the cathode planes are at ±0.5 cm.

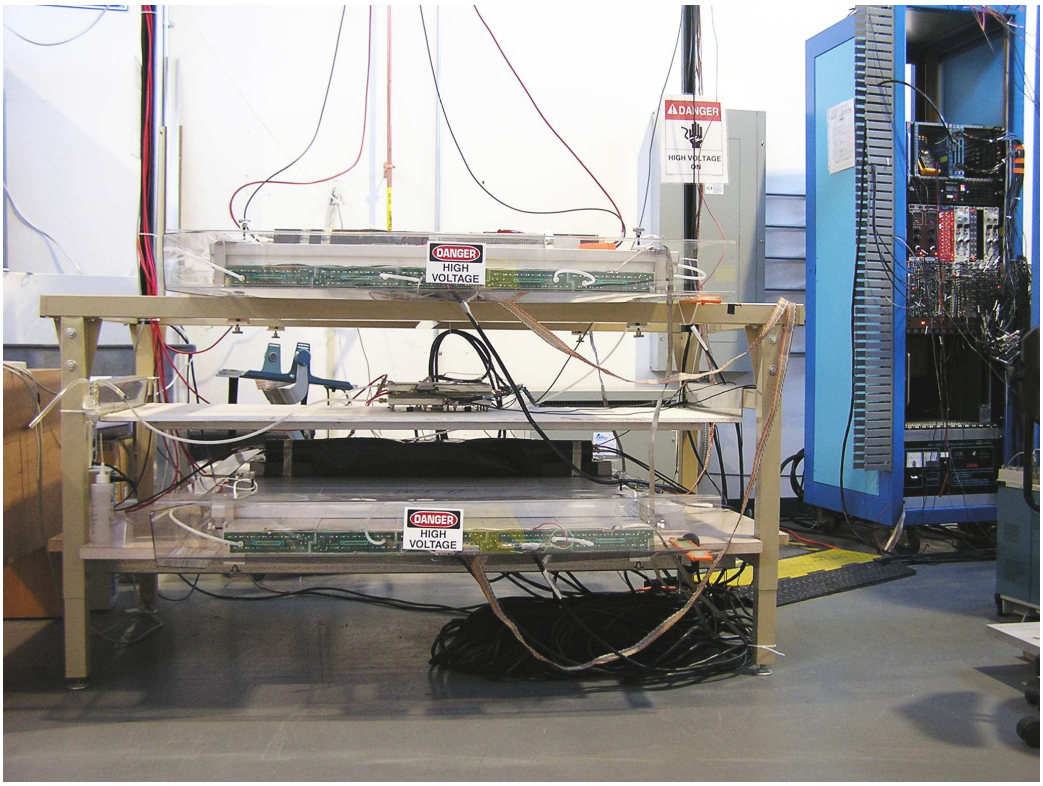

Figure 6: Photograph of test setup in the Test Lab Annex.

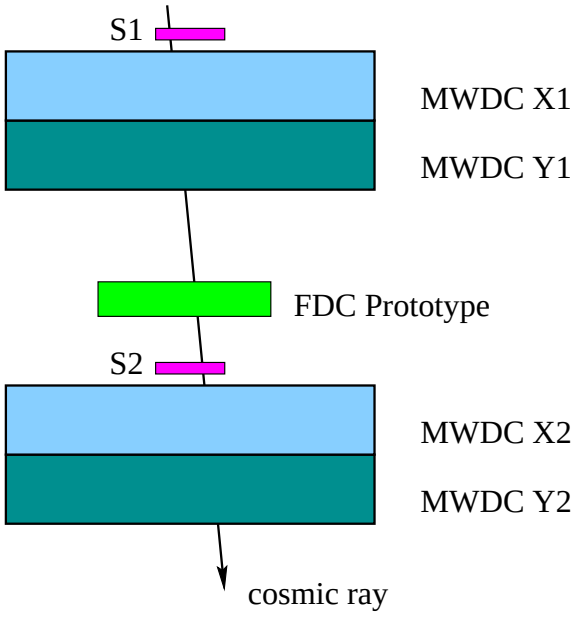

Figure 7: Schematic diagram of the cosmic ray telescope. S1 and S2 are the two trigger scintillators. Each 1-m long MWDC consists of two layers of 1-in square drift cells.

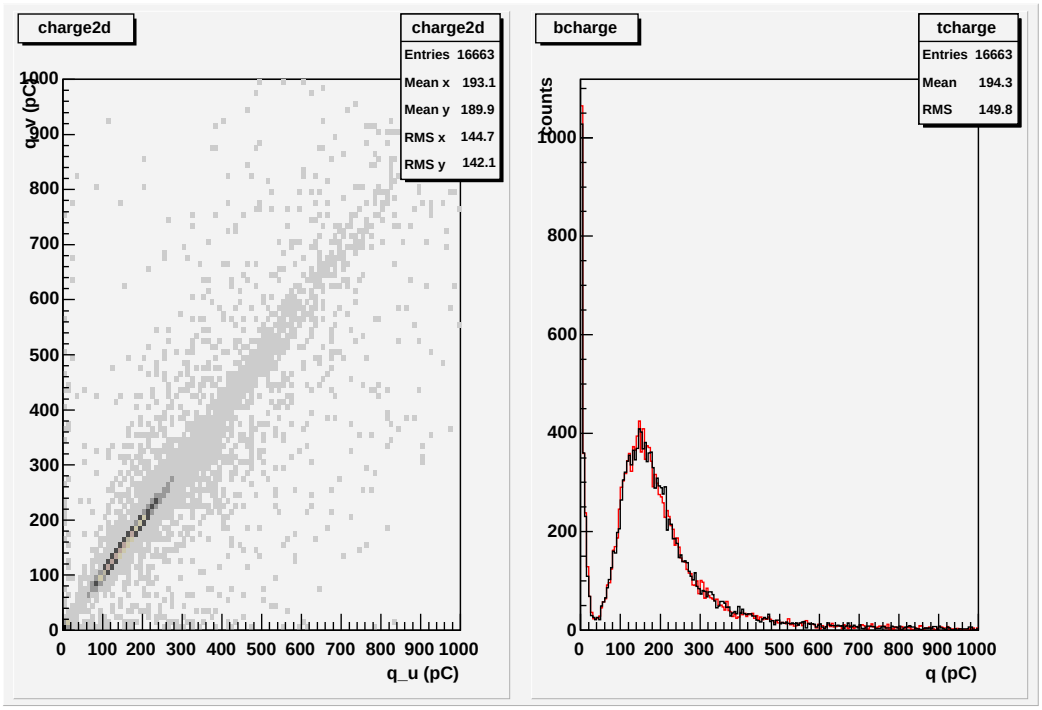

Figure 8: Charge distributions on the top (u) and bottom (v) cathodes integrating over 7 strips about the maximum in each case. The red histogram on the right is for the bottom layer, the black is for the top.

this range; see for example the peaks in figure 10). In both views there is a noise peak below 30 pC, which is a natural place to put a threshold.

A simple algorithm was implemented to count the number of peaks above a certain ADC threshold (100 channels above pedestal) in the distribution of hits on the cathode planes on an event-by-event basis. Currently the local maxima must be separated by at least one strip. As shown in figure 9, most of the time only one peak is found on each of the two cathode layers.

Unless stated otherwise, one peak per view satisfying a charge threshold of 30 pC will be required.

The distribution of the charge $\rho(\lambda)$ induced on the cathode plane is given by the empirical formula of Mathieson[2]

$$\frac{\rho(\lambda)}{q_a} = k_1 \left(\frac{1 - \tanh^2(k_2\lambda)}{1 + k_3 \tanh^2(k_2\lambda)} \right), \tag{1}$$

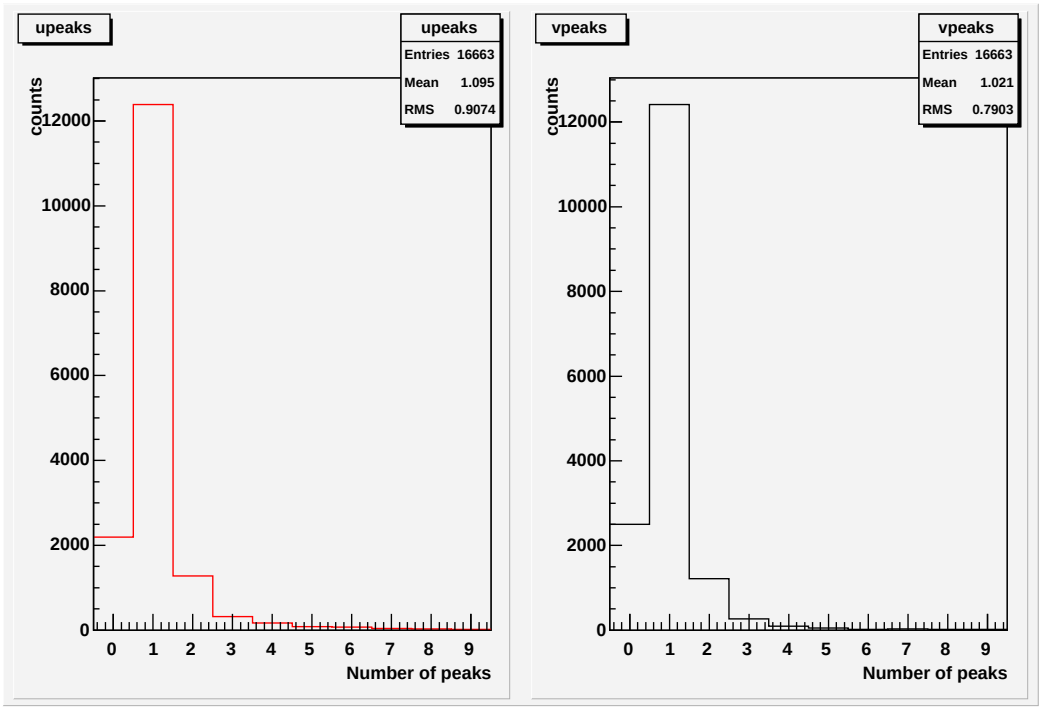

Figure 9: Distribution of the number of peaks found in u and v layers.

$$k_2 = \frac{\pi}{2}\left(1 - \frac{\sqrt{k_3}}{2}\right), \tag{2}$$

$$k_1 = \frac{k_2\sqrt{k_3}}{4\tan^{-1}\sqrt{k_3}}. \tag{3}$$

Here $\lambda = u/h$, u is the coordinate transverse to the strips relative to the center of the distribution, h is the anode-cathode gap, and q_a is the net anode charge. This functional form only depends on one parameter, which we will take to be k_3. Only the cases where the charge distribution is measured transverse to the anode wires or along the anode wire direction are treated in the literature. In Mathieson's fourth paper[2], the functional form is the same for the two cases, but the k_3 parameter is different. Here I assume that for cathode strip orientations at other angles with respect to the wires, the shape of the distribution can be described by the same empirical function with yet another choice for k_3.

Figure 10 shows a sample event showing the pedestal-subtracted ADC values for each of the two views and the results of fits to the peaks using the Mathieson function with $k_3 = 1.0$. Five strips in the top and bottom cathode layers were used in the fits for each event. Figure 11 shows the correlation between centroids measured on the u and v cathode planes. The diagonal bands correspond to the anode wires. Figure 12 shows the same information converted to the x-y coordinate system, with y along the wire and x transverse to the wires. The distribution is quantized in the x-direction (figure 13) according to the wire positions because for each event the avalanche occurs near the wire. A Gaussian fit to one of the central peaks was used to obtain a measure of the position resolution. This resolution provides a measure of the cathode resolution. The resolution of the peak at x=305 mm was 253 μm.

Figure 14 shows the dependence of the resolution on the number of strips involved per layer in the fits for the case where $k_3 = 1$. We found that the optimum number of strips is 3; the resolution gradually worsens (because more noise is introduced) as the number of strips is increased. We found that the resolution improves for larger values of k_3 and eventually levels off for $k_3 > 0.8$ (figure 15).

Table 1 lists the resolutions obtained for several of the wire positions for the case where three strips were involved in the fit and $k_3 = 1.0$.

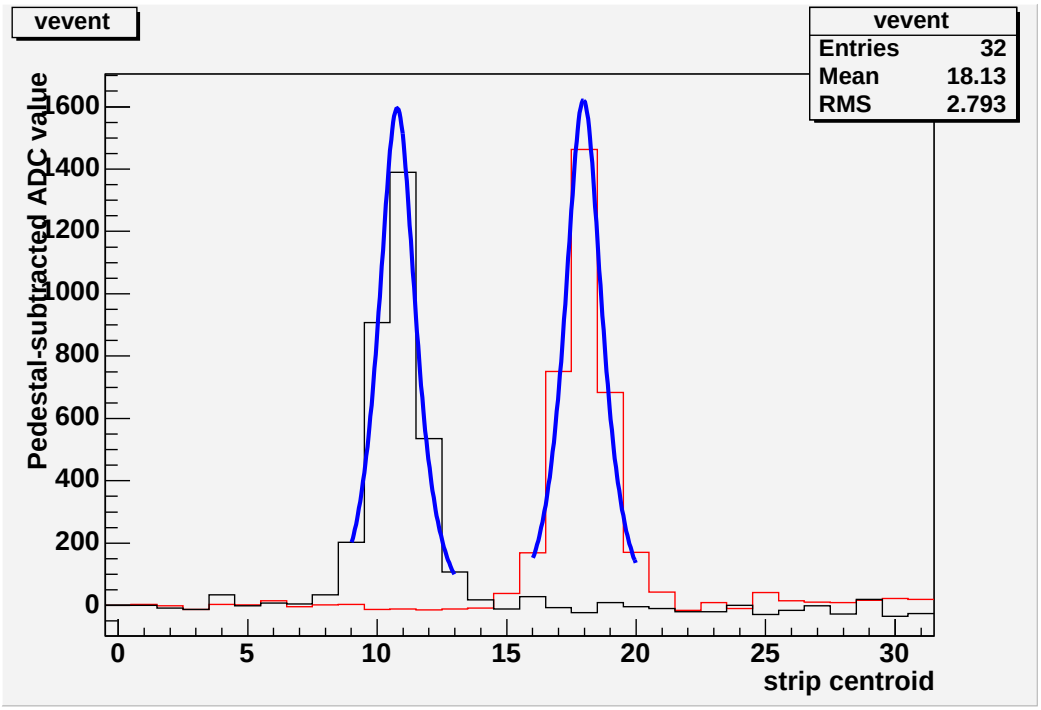

Figure 10: Sample event showing ADC signals on each of the two cathode planes. The blue curves show the results of the fits using the Mathieson function with $k_3 = 1.0$. The black histogram is for the top (u) view; the red histogram is for the bottom (v) view.

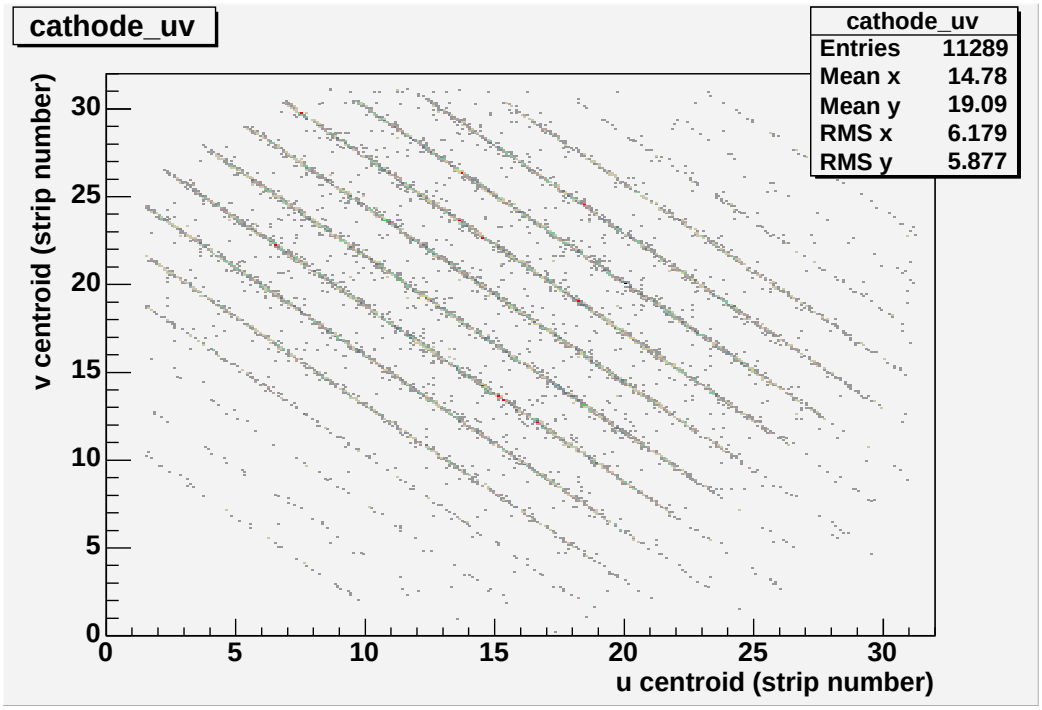

Figure 11: Correlation between centroids in u and v cathode planes.

Wire position (mm)	Resolution (μm)
265.0	202
274.9	220
284.9	212
294.9	233
304.9	253
314.9	237
324.9	244
335.0	227
344.9	218
355.0	267

Table 1: Wire positions and resolutions for the current best cathode centroid fitting parameters.

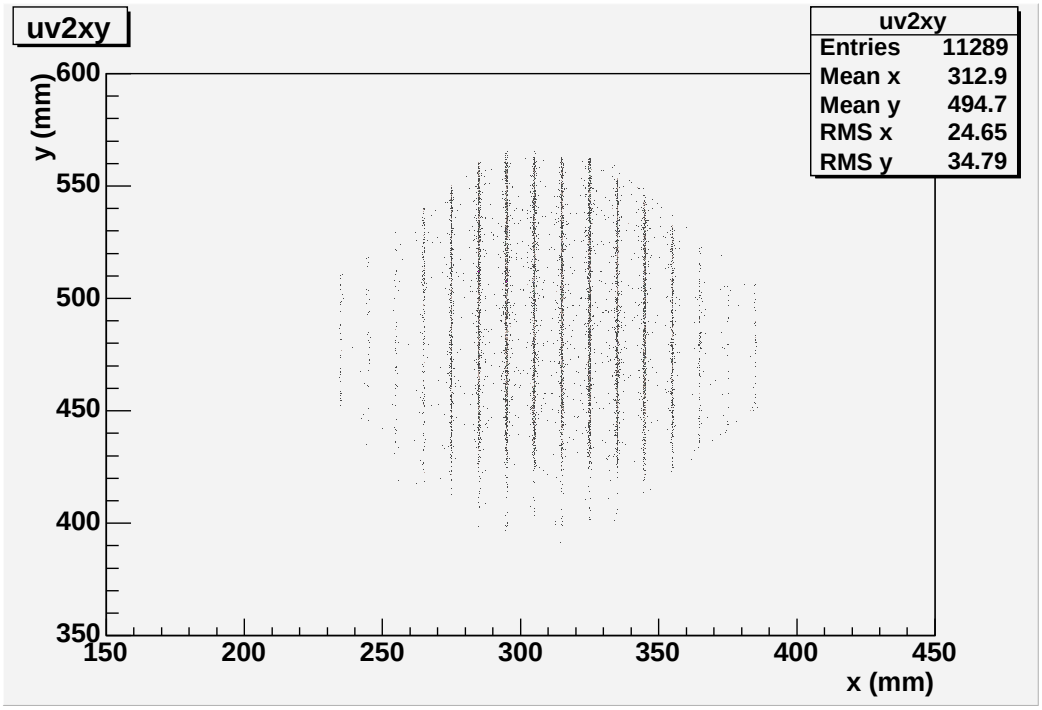

Figure 12: Hit positions of avalanches converted to x-y coordinate space.

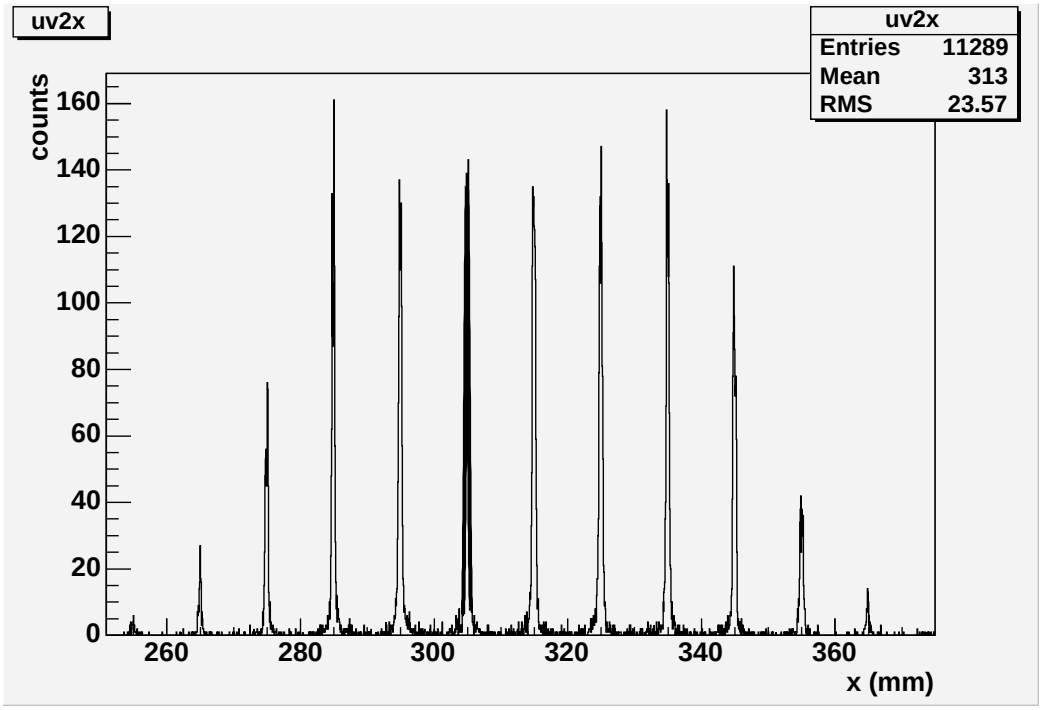

Figure 13: Reconstruction of wire positions using cathode plane information only.

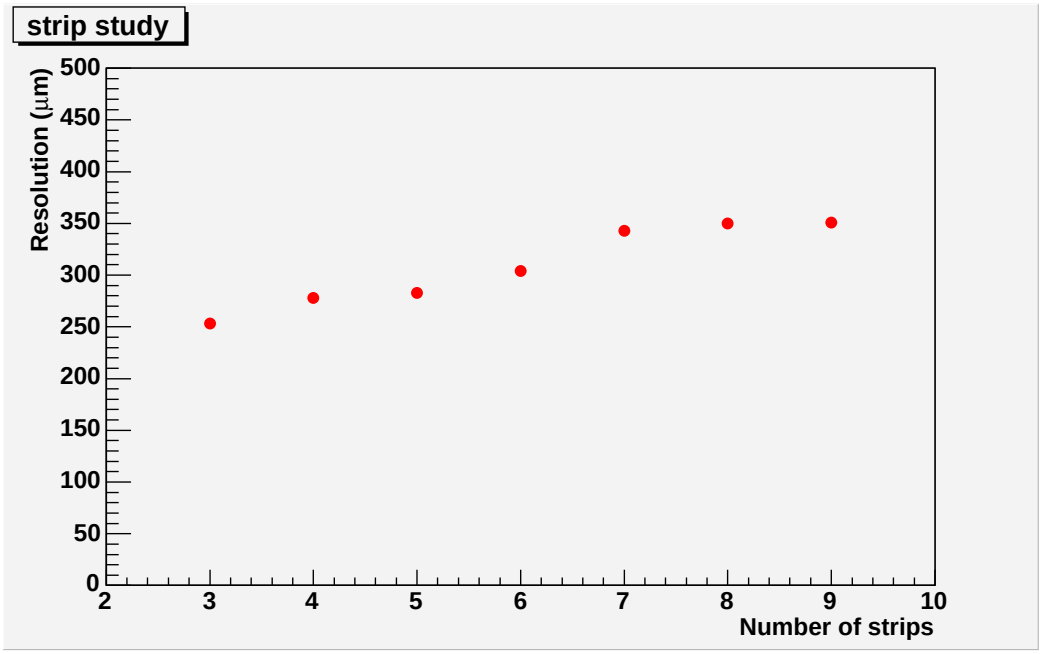

Figure 14: Dependence of resolution on number of strips per plane involved in fits. The k_3 parameter was fixed to 1.0.

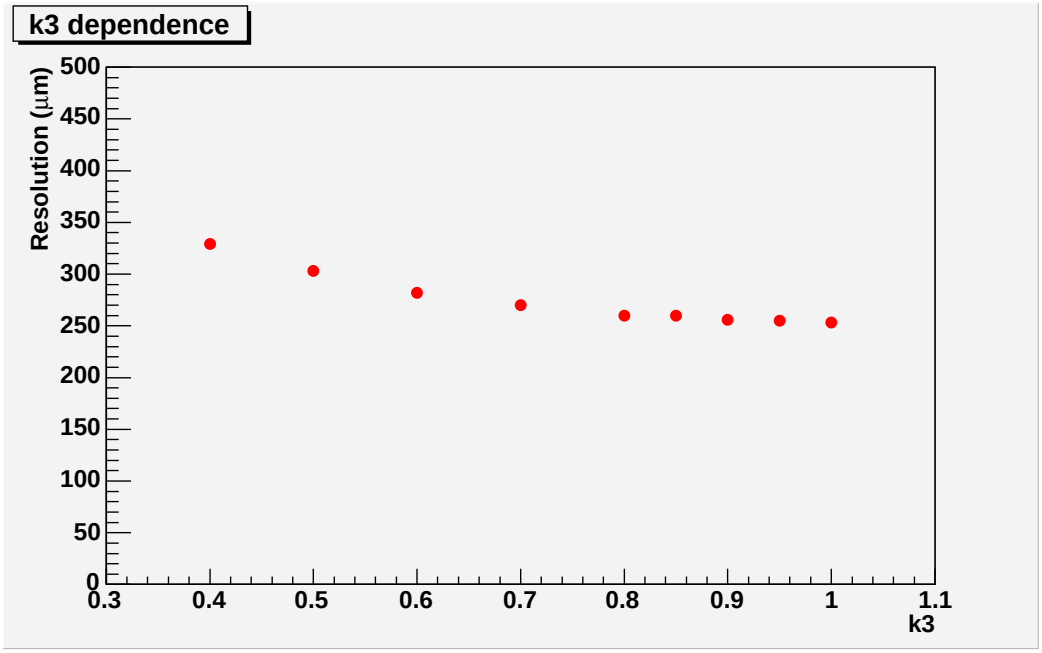

Figure 15: Dependence of resolution on the k_3 parameter. The number of strips in the centroid fit was 3.

References

[1] E. Gatti, A. Longoni, P. Semenza and H. Okuno, Nucl. Instrum. Meth. **163**, 83 (1979).

[2] E. Mathieson, Nucl. Instrum. Meth. A **270**, 602 (1988).